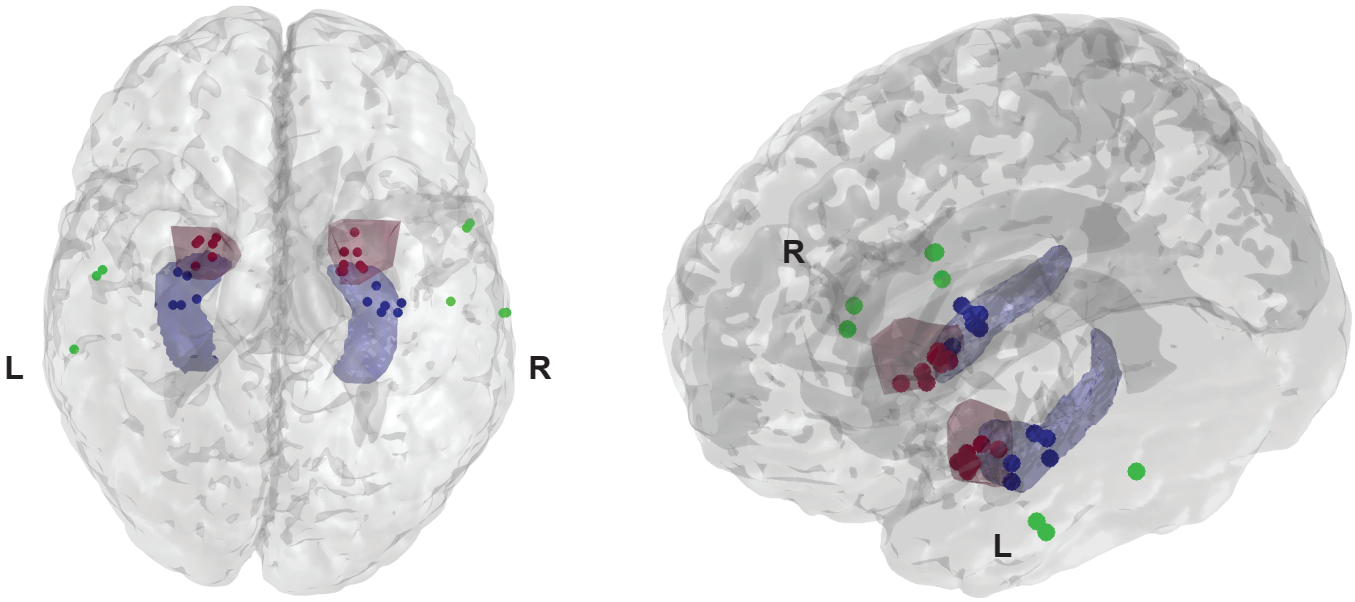

Figure S1. Recording locations. Related to Figure 1.
Electrodes across all subjects. Red, PCx; blue, AH; green, lateral temporal cortex (LTC). LTC was used as a control region for analysis of cross-structural theta synchrony during replay events. See also **Table S1** for MNI coordinates of all included electrodes.

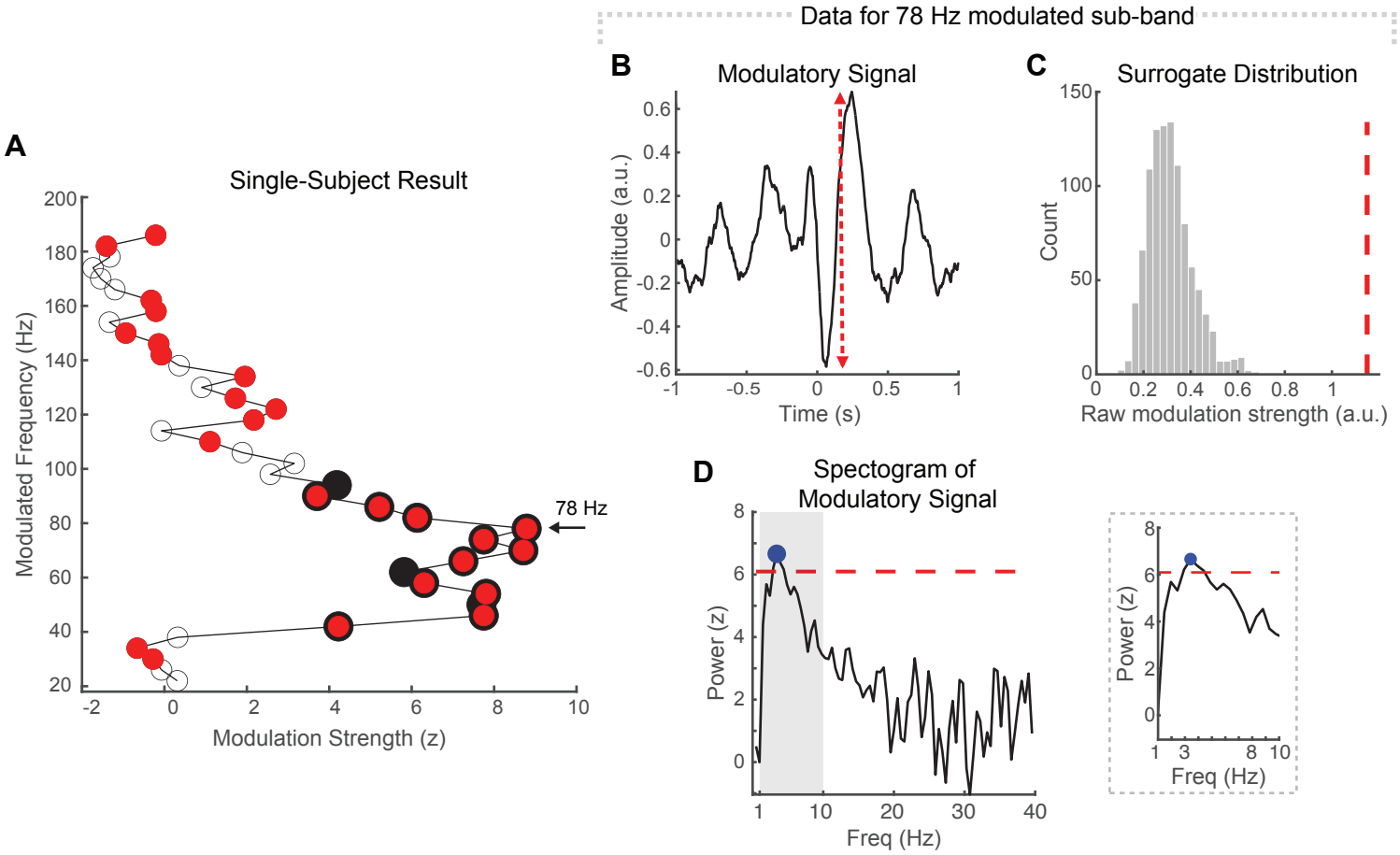

Figure S2. PAC method schematic. Related to Figure 2B.
(**A**) PAC was assessed across a broad range of potential frequencies for the modulating (1-10 Hz) and modulated (20-200 Hz) oscillations. Single-subject PAC results are shown with data from AH. Pooling trials across encoding (cue 1/2/3) and maintenance (see Methods), modulation strength was quantified independently for each of the 42 modulated sub-bands spanning 20 to 200 Hz (bandwidths linearly scaled from 6 to 50 Hz). Larger black circles indicate significant modulation strength (corrected across modulated sub-bands, $p < 0.025$), whereas smaller red circles indicate that the predominant modulating frequency was within the theta frequency range. In this subject, eleven sub-bands within the gamma frequency range (i.e., 20-100 Hz) demonstrated significant coupling with theta, for which the specific frequencies ranged between 3.0 and 4.4 Hz, with maximal coupling at 78 Hz (arrow). (**B-D**) We illustrate how modulation strength and modulating frequency were determined for each evaluated modulated sub-band, using data from the 78 Hz sub-band. (**B**) In the 78 Hz bandpass-filtered signals of each trial, we identified periods of enhanced activity (max power > 2 s.d. above the mean of the pre-encoding baseline) that was sustained for > 3 oscillatory cycles. These events were used as trigger time points to compute the modulatory signal, which is the average of the raw peri-event LFP signals ([-1, 1] s). The maximum peak-to-trough distance of the modulatory signal (red dashed arrows) represents the raw modulation strength. (**C**) For statistical testing, this procedure was repeated for time points randomly selected from the entire experimental trace. The resulting distribution of surrogate modulation strengths was used to *z*-score normalize the observed modulation strength (red dashed line). (**D**) Oscillatory peaks were identified from the spectrogram of the modulatory signal (see Methods; see also **Figure S3A-B**). A modulating frequency was reported if the local maximum was within the frequency range of interest (i.e., 1-10 Hz; indicated by gray shade, also shown within gray dashed box), and satisfied a threshold criterion of 2 s.d. greater than the mean (red dashed line; suprathreshold peak indicated by blue circle). In this subject, there a clear peak within the theta band at 3.4 Hz, which was congruent with the center frequencies identified from the power spectra of encoding and maintenance task periods (see **Figure S3D**, AH panel, S7 in black).

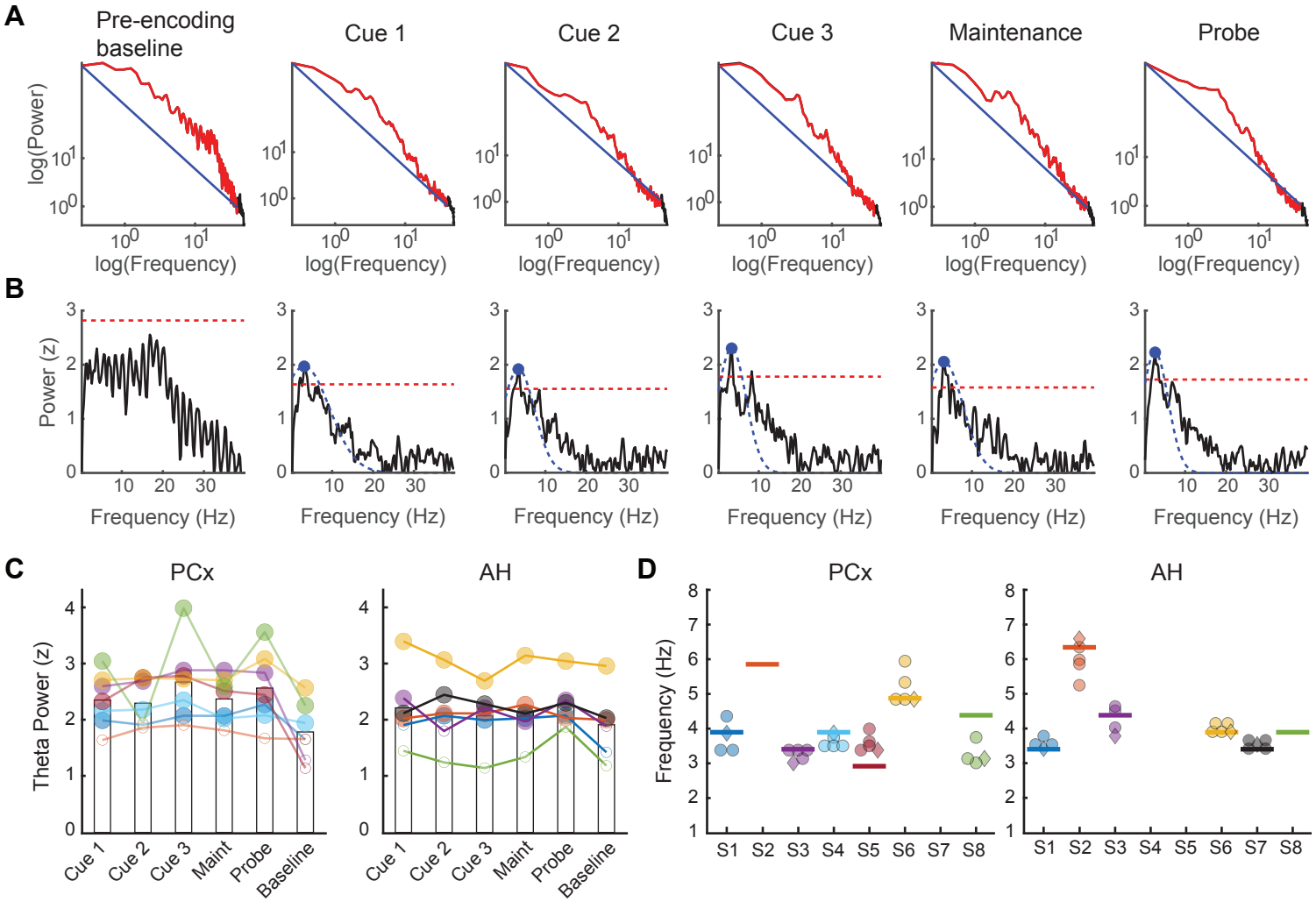

Figure S3. Single-subject illustration of theta power analysis with spectrograms (A-B), group-level theta power (C), and comparison of theta frequencies at peak power vs. at maximal coupling with gamma oscillations (D). Related to Figure 2C-D.

(**A-B**) Single-subject results shown with data from PCx. (**A**) Spectrograms of each task period as well as the pre-encoding baseline are shown in log-log space. The aperiodic portion of the signal was initially fitted (blue) over the frequency range 0.1 to 40 Hz (red portion of black trace). (**B**) The fit of the aperiodic portion was removed, where the residual signal is assumed to be mix of oscillatory peaks and noise. The residual was then *z*-score normalized with respect to itself (black), and oscillatory peaks were identified with a threshold criterion of 2 s.d. greater than the mean (red dashed line; suprathreshold peaks indicated by blue circles), which were then fitted with a Gaussian (blue dashed line). The fitted Gaussian was removed, and this process is repeated until all suprathreshold oscillatory peaks are identified and removed. In this subject, a secondary peak was found at 12 Hz only for Cue 2 (see Methods). Note that there were no oscillatory peaks identified during baseline. Finally, we returned to the raw spectrogram, from which Gaussian fits of all oscillatory peaks, if any, are removed, and a final fit of the aperiodic component is performed in log-log space. The slope of the aperiodic portion was consistent across task periods ([-1.45, -1.33]). The overall fit of the spectrogram (both the aperiodic portion and any oscillatory peaks) was then assessed with the *F*-test (in this subject, $p < 10^{-24}$ for task periods, $p < 10^{-15}$ for baseline). For the power and center frequencies of theta-band peaks, we reported the height and frequency at the local maximum (blue circles), respectively. If no theta-band peaks were identified, we only reported power (and not the center frequencies), for which we presented the height at the local maximum within the theta frequency range. (**C**) In this way, theta power in each task period and the pre-encoding baseline period was quantified. Within subjects, there was no difference in theta power across task periods in either region of interest

(one-way ANOVA; $p > 0.6$). Larger solid circles (vs. smaller empty circles) indicate supra-threshold theta power. (**D**) Within subjects, the center frequencies of theta-band peaks in the spectograms were consistent across task periods (one-way ANOVA; $p > 0.8$). For each subject, we also show the modulating frequency associated with the greatest modulation of gamma bursts throughout encoding and maintenance (horizontal lines), which were all within the theta frequency range (see Methods; see also **Figure S2**). Within subjects, this modulating frequency was consistent with the center frequencies of theta peaks identified from spectrograms of encoding (cue 1/2/3) and maintenance task periods (circles; data from retrieval period marked separately with diamonds). Note that S7 had no data from PCx; S4 and S5 had no data from AH. Frequency data not shown for S2 in PCx and S8 in AH, as supra-threshold theta peaks were not identified.

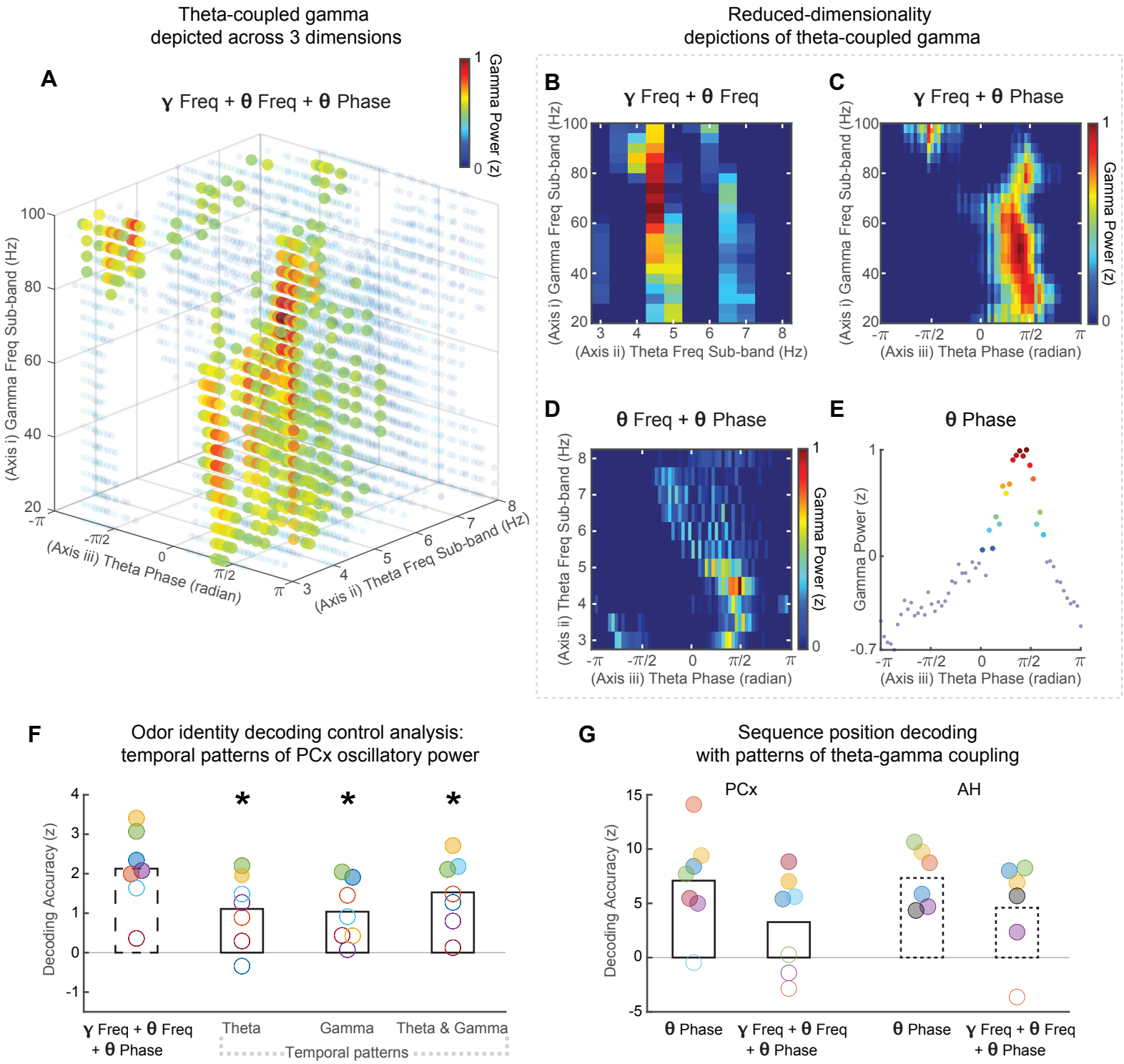

Figure S4. Feature space formats depicting the pattern of theta-coupled gamma (A-E), odor identity classification with temporal patterns of oscillatory power (F), odor sequence position classification with patterns of theta-coupled gamma (G). Related to Figure 4.
(**A-E**) Example of a single-trial PCx response to a cue odor. (**A**) The full feature space describes the pattern of cue odor-induced theta-coupled gamma activity across three axes: i. gamma frequency sub-band, ii. theta frequency sub-band, and iii. theta phase. Information along one or more of these axes was selectively eliminated ("lesioned") to construct alternate feature spaces depicting the pattern of theta-coupled gamma, but with reduced dimensionality: (**B**) gamma frequency + theta frequency (retains axes i and ii); (**C**) gamma frequency + theta phase (retains axes i and iii); (**D**) theta frequency + theta phase (retains axes ii and iii); and (**E**) theta phase (retains axis iii only). Note that the information in feature space (**E**) was used to demonstrate

theta phase coding of sequence position. For visualization, gamma power was thresholded above the mean and relatively scaled across features spaces. (**F, G**) For each feature space, we show each subject's normalized decoding accuracy. Solid circles (vs. empty) indicate significant decoding (surrogate test, $p < 0.05$). (**F**) To further validate that the full three-dimensional pattern of theta-coupled gamma carried the most relevant information for PCx odor coding, classification was attempted using the temporal pattern (relative to stimulus onset) of odor-induced oscillatory power in the theta band, gamma band, or both (solid bars). For comparison, decoding results using the three-dimensional theta-coupled gamma feature space (dashed bars) are replicated here (from **Figure 4**). While odor identity could be decoded with temporal patterns of oscillatory power in a subset of subjects, model performance was superior with the three-dimensional theta-coupled gamma feature space (paired-sample *t*-test, $*p < 0.05$). Raw decoding accuracy was, from left to right, 13.9 ± 0.4%, 12.7 ± 0.3%, 12.4 ± 0.2%, and 13.3 ± 0.4% (chance level accuracy = 10%). (**G**) Sequence position was decoded from single-trial responses to cue odors in PCx (solid bars) and AH (dotted bars), using the set of sequence-correct trials only. Classification with the reduced dimension feature space depicting the pattern of gamma across theta phase only (feature space **E**) was significant in six subjects (out of seven) in PCx, and in all six subjects in AH. Raw decoding accuracy was 47.0 ± 3.4% in PCx, and 46.4 ± 1.6% in AH (chance = 33%). Model performance with the full three-dimensional feature space (feature space **A**) did not lead to superior decoding ($p > 0.2$; raw decoding accuracy 40.1 ± 3.5% in PCx, 41.3 ± 3.2% in AH). These results suggest that sequence position is conveyed by the theta phase specificity of theta-coupled gamma, and less so by the specific sub-bands within theta and gamma that are coupled, which is consistent with a theta phase code of temporal order information.

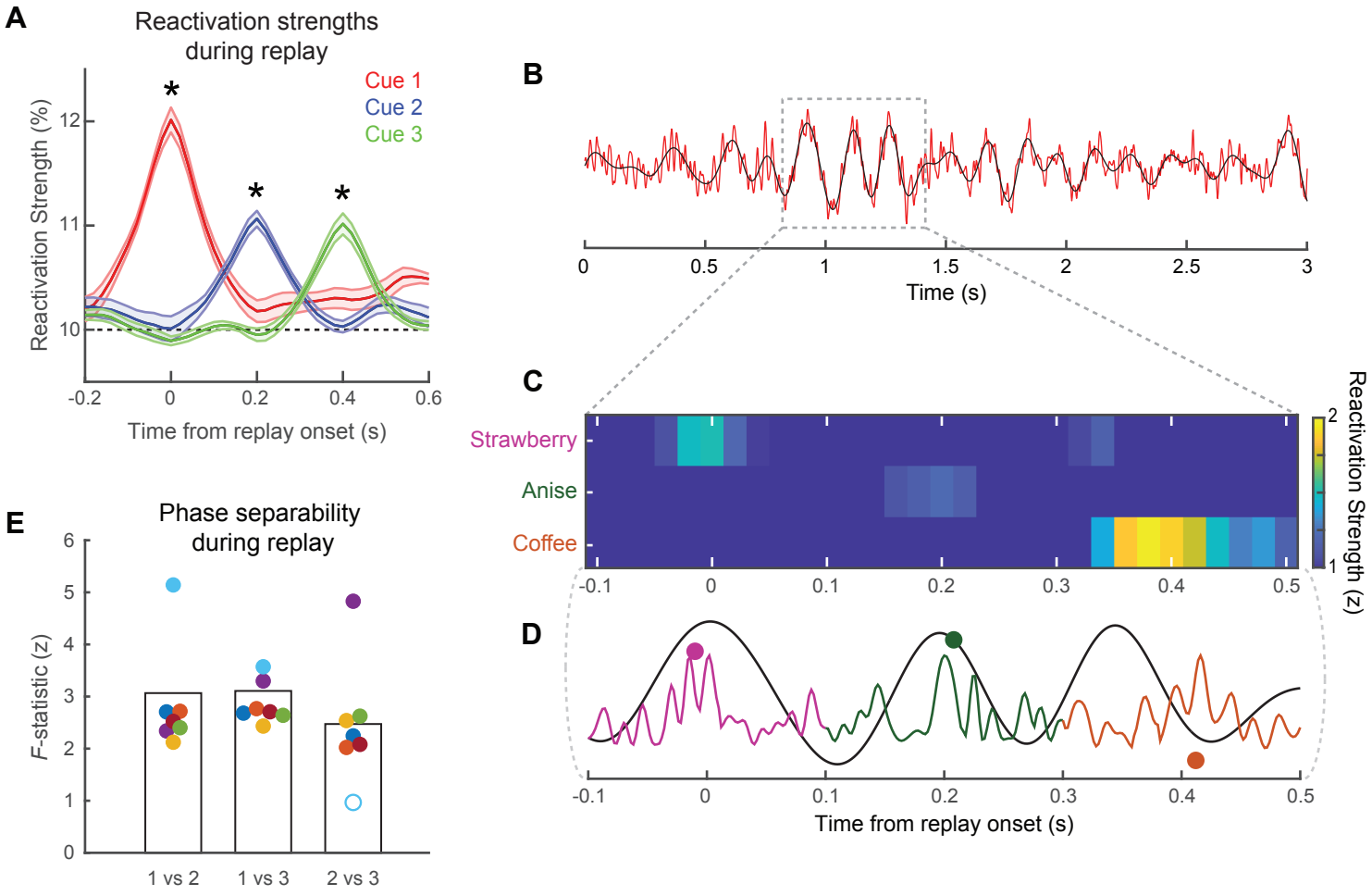

Figure S5. Group-level replay event (A) and phase separability during replay (B-E). Related to Figure 6.

(**A**) Subject-averaged cue odor reactivation strengths during replay events identified for an inter-reactivation time lag of 200 ms (see Methods). Reactivation strengths for the first, second, and third cues were greatest at replay onset, 200 ms, and 400 ms, respectively (paired-sampled *t*-test, $*p < 10^{-3}$). Horizontal dashed line indicates chance-level reactivation strength; shading indicates s.e.m. across subjects. (**B-D**) We illustrate our method to assess phase separability of cue odor reactivations during replay, using data from a single replay event. (**B**) A single-trial example of PCx delay activity is shown, in which the raw LFP was bandpass-filtered in the theta (black) and gamma (red) bands (relatively scaled for visualization). Time-resolved decoding analysis revealed memory replay beginning ~ 900 ms into the trial epoch (gray dashed box). For this replay event, we show the reactivation strengths of each cue odor (**C**), and also the baseline-normalized gamma power during each cue odor reactivation (**D**; theta-filtered signal overlaid in black, relatively scaled). The preferred theta phase during each cue odor reactivation (solid circles) was determined by dividing the replay event into three temporal epochs, and computing the distribution of gamma power across theta phase bins (see Methods). (**E**) The preferred theta phases of individual cue odor reactivations across all replay events were then compared between each unique pair of sequence positions (position 1 vs. 2, 2 vs. 3, 1 vs. 3) with the Watson-William test. Data is shown after the observed *F*-statistic was *z*-score normalized with respect to surrogate data obtained by repeating the analysis on randomly sampled time windows, as opposed to during replay events (see Results). Solid circles indicate significance ($p < 0.05$); colors indicate individual subjects.

	Piriform cortex	Anterior hippocampus	Lateral temporal cortex
S1	(19 -2 -25); (23 -2 -24)	(37 -17 -15); (32 -18 -15)	(52 -16 -16)
S2	(-20 1 -25); (-25 0 -25)	(-31 -9 -20); (-32 -20 -20)	(-56 -12 -27)
S3	(24 -6 -21); (19 -6 -20)	(31 -20 -19); (36 -20 -19)	(71 -19 -18)
S4	(22 4 -26); (18 -8 -19)		(57 8 -30)
S5	(20 -8 -19); (25 -8 -21)		(73 -19 -19)
S6	(-22 -6 -20); (-27 -8 -19)	(-25 -18 -16); (-30 -20 -16)	(-62 -35 -9)
S7		(29 -11 -22); (-28 -10 -28)	(-54 -10 -30)
S8	(-22 -1 -22); (-27 -1 -22)	(27 -17 -14); (31 -20 -15)	(56 7 -22)

For each electrode, numbers indicate (X Y Z) coordinates.

Table S1. Montreal Neurological Institute (MNI) coordinates of electrodes in regions of interest. Related to Figure 1A.